Research Article

Sohail Ahmad*, Kashif Ali, Muhammad Ashraf, Hamiden Abd El-Wahed Khalifa, Fayza Abdel Aziz ElSeabee, and El Sayed M. Tag El Din

Analysis of pure nanofluid (GO/engine oil) and hybrid nanofluid (GO–Fe_3O_4/engine oil): Novel thermal and magnetic features

https://doi.org/10.1515/ntrev-2022-0486
received May 28, 2022; accepted September 16, 2022

Abstract: Hybrid nanofluids can provide better physical strength, thermal conductivity, and mechanical resistance in many thermodynamic systems than pure nanofluids. To establish the novel results, using superior types of hybrid nanoparticles like graphene oxide (GO) and iron oxide (Fe_3O_4) is the main focus of recent work. This study investigates the innovative thermal and magnetic features of both pure nanofluid GO/engine oil (EO) and hybrid nanofluid GO–Fe_3O_4/EO under the simultaneous effects of induced as well as applied magnetic field. The chemical reaction phenomenon together with activation energy has also been taken into account. A novel algorithm based on order reduction and finite difference discretization is developed in order to numerically treat the problem. The efficiency of the code is appraised by a numerical comparison which is found to be in a good correlation with the existing results. From the consequences of this study, it is deduced that the reduction in induced magnetic field and fluid's velocity (in case of either pure or hybrid nanofluid) is associated with the enlarging values of magnetic Prandtl number and induced magnetic field parameter. Further, activation energy is responsible for enhancement in concentration. The hybrid nano-composition of GO–Fe_3O_4/EO can provide the thermal stability, prevent the corrosion and make the liquid to stay in high temperature.

Keywords: graphene oxide, iron oxide, engine oil, activation energy, induced magnetic field

*** Corresponding author: Sohail Ahmad,** Centre for Advanced Studies in Pure and Applied Mathematics (CASPAM), Bahauddin Zakariya University, Multan-60800, Pakistan; Department of Basic Sciences and Humanities, Muhammad Nawaz Sharif University of Engineering and Technology, 60000, Multan, Pakistan, e-mail: sohailkhan1058@gmail.com
Kashif Ali: Department of Basic Sciences and Humanities, Muhammad Nawaz Sharif University of Engineering and Technology, 60000, Multan, Pakistan
Muhammad Ashraf: Centre for Advanced Studies in Pure and Applied Mathematics (CASPAM), Bahauddin Zakariya University, Multan-60800, Pakistan
Hamiden Abd El-Wahed Khalifa: Department of Operations Research, Faculty of Graduate Studies for Statistical Research, Cairo University, Giza 12613, Egypt; Department of Mathematics, College of Science and Arts, Qassim University, Al-Badaya 51951, Saudi Arabia
Fayza Abdel Aziz ElSeabee: Mathematics Department, Faculty of Science, Helwan University, Cairo, Egypt; Department of Mathematics, College of Science and Arts, Alasyah, Qassim University, Saudi Arabia
El Sayed M. Tag El Din: Department of Electrical Engineering, Faculty of Engineering and Technology, Future University in Egypt, New Cairo 11835, Egypt

Nomenclature

$\vec{B_0}$	uniform magnetic field
c	stretching/shrinking constant
C	concentration of the fluid
C_∞	concentration far away from the sheet
$C_{p_{\mathrm{hnf}}}$	specific heat of hybrid nanofluid
D_B	diffusion coefficient
E^*	activation energy
H_1	induced magnetic field component along x-axis
H_2	induced magnetic component along y-axis
H_e	magnetic field at the edge of boundary layer
k^*	Darcy permeability
K_r	rate constant of chemical reaction
k_{hnf}	thermal conductivity of hybrid nanofluid
m_1	exponent fixed rate
T	temperature of the fluid
T_∞	temperature far away from the sheet
T_w	fixed temperature at the surface
u	component of velocity along x-axis
v	component of velocity along y-axis
v_0	suction velocity (where $v_0 > 0$)

υ_{hnf} kinematic viscosity of hybrid nanofluid
μ_e magnetic permeability
μ_{hnf} hybrid nanofluid viscosity
σ_{hnf} electrical conductivity of hybrid nanofluid
ρ_{hnf} density of hybrid nanofluid

1 Introduction

The combination of different nanoparticles possesses superior thermal features which have several practical employments in modern engineering and technology. Usually hybrid nanofluids are prepared by mixing two or more distinct nanoparticles with the base fluid. This combination yields a homogeneous compound which involves different characteristics as compared to individual nanoparticles. Metal base nanoparticles like aluminum oxide (Al_2O_3), cerium oxide (CeO_2), zinc oxide (ZnO), titanium dioxide (TiO_2), and iron oxide (Fe_3O_4) play a crucial role in augmentation of heat transfer in many systems. The iron oxide nanoparticles such as Fe_3O_4 are natural compounds which can also be synthesized in the laboratory. Due to their super magnetic properties, the magnetite particles Fe_3O_4 are used widely in magnetic ink and toner, rubber, plastic, paper, glass, ceramic glazes, and cosmetics as well as in textiles. In the same way, graphene oxide (GO) is a lightweight and thin nanomaterial or compound which is made of carbon, hydrogen, and oxygen. It is a promising nanomaterial having several applications in medicine and biotechnology for drug delivery, cancer treatment, and cellular imaging. The engine oil (EO) based hybrid nano-composite of Fe_3O_4 and GO might be of great interest in thermal heating and cooling systems.

The involvement of magnetite nanoparticles in hybrid or non-hybrid nanofluids is important due to their super paramagnetic properties. In this regard, a lot of work has been performed by many researchers. A magnetized non-Darcy flow of hybrid nanofluid (MWCNT + Fe_3O_4/water) subject to convective boundary conditions was explored by Shah *et al.* [1]. The control volume finite element computational technique was adopted to determine the numerical solution. This thermally conductive flow was strengthened due to Lorentz force and porosity of the medium. Tekir *et al.* [2] investigated the water-based hybrid nanofluid flow involving Fe_3O_4 and copper (Cu) as nanoparticles. The flow was taken within a straight pipe under the effect of constant magnetic field. The range of parameters like Reynolds number and solid nanoparticles volume fraction was adjusted in such a way that increased Nusselt number may be obtained (*e.g.*, $0 < \varphi < 0.02$ and $994 < \mathrm{Re} < 2{,}337$). The features of mono nanofluid $MnZnFe_2O_2/H_2O$ as well as hybrid nanofluid $MnZnFe_2O_2$–$NiZnFe_2O_2/H_2O$ together with gyrotactic microorganisms were elaborated by Ahmad *et al.* [3]. In this study, it was found that the heat transfer rate increased significantly with the composition of zinc ferrites and motile gyrotactic microorganisms. The ferrofluid-based magnetite nanomaterials (Fe_3O_4) were evaluated in order to reduce the viscosity of oil ([4]). They utilized engine lubricant oil to synthesize the carrier fluid. Astafyev *et al.* [5] used the thermomagnetometric method to study the nickel–zinc ferrites taking different magnetic phase transitions.

Hemmat Esfe *et al.* [6] described the rheological behavior of hybrid nanofluid (MWCNT–Al_2O_3) based on temperature, volume fraction of nanoparticles, and shear rate to present an experimental correlation model. Vidhya *et al.* [7] experimentally and statistically reported the convective heat transfer performance of a cylindrical mesh-type heat pipe apparatus filled with ZrO_2–CeO_2/water–ethylene glycol nanofluids. Thermal conductivity and viscous properties of water-based SiO_2–ND hybrid nanofluid were measured experimentally by Yalçın *et al.* [8]. The flow over a curved surface was interpreted by Mishra and Upreti [9] to check out the effects of ethylene glycol based hybrid nanofluids $CoFe_2O_4$–Fe_3O_4/water on heat transfer characteristics. Jan *et al.* [10] mixed the inorganic nanomaterials such as Cobalt (Co) and Fe_3O_4 to prepare the hybrid nano composition of Co–Fe_3O_4/$C_2H_6O_2$–water. They found the numerical solution of the problem using BVP4c built in function in Mathematica. Magnetically driven flow of EO comprising Cu and titanium oxide was numerically examined by Ali *et al.* [11] by employing Quasi–linearization method. Yu *et al.* [12] used commercially available nanomatrerials *e.g.*, $H_2C_2O_4{\cdot}2H_2O$, $NiSO_4{\cdot}6H_2O$, $ZnSO_4{\cdot}7H_2O$, and $FeSO_4{\cdot}7H_2O$ to analyze their thermal properties. Their outcomes portrayed that the ferrites such as Ni–Zn demonstrated better magnetic properties which could be beneficial in microwave absorbers. An experimental study was presented by Azhagushanmugam *et al.* [13] in which the effect of nanoparticles nickel cobalt zinc ferrites (Ni–Co–$ZnFe_2O_4$) on concentration and magnetization was examined. Further recent investigations on mono and hybrid nanofluids can be seen in refs [14–20].

In order to initiate the chemical or biochemical processes, certain amount of energy is always required. A small quantity of energy which is required to accelerate the chemical reaction process is known as activation energy. Bestman [21] presented, for the first time, the

idea of boundary layer flow consisting of activation energy. He adopted perturbation technique to numerically solve this problem. A numerical technique named RKF-45 was implemented by Ramesh and Madhukesh [22] and Madhukesh *et al.* [23] to numerically interpret the hybrid nanofluid flows through extendable slipped surface and circular cylinder, respectively. The flow of Williamson fluid involving Al_2O_3 and Cu under the heterogeneous and homogeneous chemical reactions was deliberated by Almaneea [24]. It was disclosed that the Cu–Williamson nanofluid was marginally affected by the Lorentz force as compared to Cu–Al_2O_3–Williamson hybrid nanofluid. Rekha *et al.* [25] proposed hybrid nanoparticles like aluminum alloys (AA7075 and AA7072) to prepare the water-based hybrid nanofluids. They investigated the flow and thermal features in the presence of activation energy by taking different geometries (plate, wedge, and cone).

The EO-based magnetized hybrid nanoparticles not only control the temperature but can also act as cooling fluid. The composition of GO–Fe_3O_4/EO can provide thermal stability, prevent corrosion, and make the liquid to stay in high temperature. The flow of EO together with hybrid nanoparticles (Fe_3O_4 and GO) might be used in engine cooling to maintain the viscosity-temperature properties, to protect against corrosion, and many more. Due to these interesting characteristics, we intend to investigate the novel aspects of the hybrid nanofluid which is GO–Fe_3O_4/EO in the present case. We distinguish our work from the existing literature as: (i) the combination of the proposed hybrid nanoparticles GO and Fe_3O_4 together with base fluid EO has not been reported yet; (ii) the simultaneous effect of induced as well as applied magnetic field has also been taken into account; (iii) our analysis covers the features of both GO/EO which is a mono nanofluid and GO–Fe_3O_4/EO which is a hybrid nanofluid; (iv) the role of suction, chemical reaction, and activation energy has also been discussed in either case of nanofluids.

2 Formulation of model problem

The composition of GO and magnetic Fe_3O_4 is used in EO to prepare hybrid nano-composite of GO–Fe_3O_4/EO. The components of induced magnetic field are represented by $\vec{H_1}$ and $\vec{H_2}$ while $\vec{H} = (\vec{H_1}, \vec{H_2})$ is the induced magnetic field vector. The y-axis is vertical to the surface, while direction of flow is along the x-axis. The structure of extending surface is shown in Figure 1. The concentration

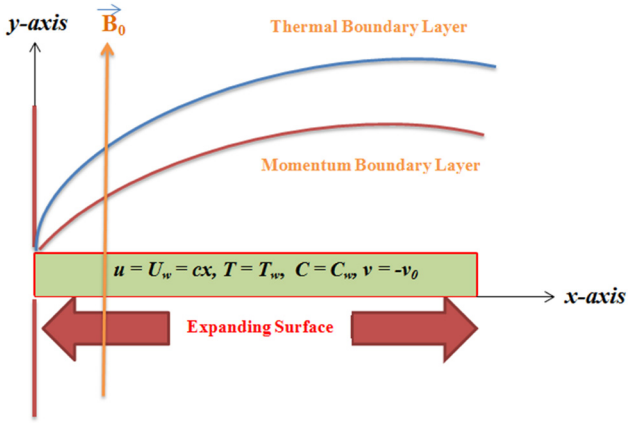

Figure 1: Structure of the geometry.

and temperature, away from surface of sheet, are expressed as C_∞ and T_∞, respectively. Likewise, C_w and T_w denote, respectively, the concentration and temperature on the surface boundary. The applied magnetic field B_0 is assumed normal to the surface (parallel to the y-axis). The surface is being stretched with a velocity $U_w(x)$. The activation energy term is also included in the concentration.

Taking into consideration the above suppositions, the flow model governing equations have the form [26,27]:

$$\frac{\partial u}{\partial x} + \frac{\partial v}{\partial y} = 0, \tag{1}$$

$$u\frac{\partial u}{\partial x} + v\frac{\partial u}{\partial y} = \upsilon_{\text{hnf}}\frac{\partial^2 u}{\partial y^2} - \frac{\sigma_{\text{hnf}}}{\rho_{\text{hnf}}}B_0^2 u + \frac{\mu_e}{4\pi\rho_{\text{hnf}}}\left(H_1\frac{\partial H_1}{\partial x} + H_2\frac{H_1}{\partial y}\right) - \frac{\mu_e H_e}{4\pi\rho_{\text{hnf}}}\frac{\partial H_e}{\partial x}, \tag{2}$$

$$u\frac{\partial H_1}{\partial x} + v\frac{H_1}{\partial y} = H_1\frac{\partial u}{\partial x} + H_2\frac{\partial u}{\partial y} + \frac{1}{4\pi\rho_{\text{hnf}}\mu_e}\frac{\partial^2 H_1}{\partial y^2}, \tag{3}$$

$$u\frac{\partial T}{\partial x} + v\frac{\partial T}{\partial y} = \frac{K_{\text{hnf}}}{(\rho C_p)_{\text{hnf}}}\frac{\partial^2 T}{\partial y^2}, \tag{4}$$

$$u\frac{\partial C}{\partial x} + v\frac{\partial C}{\partial y} = D_B\frac{\partial^2 C}{\partial y^2} - K_r^2(C - C_\infty)\left(\frac{T}{T_\infty}\right)^{m_1}\exp\left(\frac{-E^*}{k^*T}\right), \tag{5}$$

The supposed boundary conditions at the sheet surface and far away from the surface are:

$$\left.\begin{aligned} &y = 0: \quad u(x,0) = cx = U_w(x),\ T(x,0) = T_w,\\ &C(x,0) = C_w,\ v(x,0) = -v_0,\ \frac{\partial H_1}{\partial y} = H_2 = 0\\ &y \to \infty: \quad u(x,\infty) = 0, \quad T(x,\infty) = T_\infty,\\ &H_1 = H_2 = 0,\ C(x,\infty) = C_\infty \end{aligned}\right\}, \tag{6}$$

In the above relations, the velocity $v_0 > 0$ represents the suction, the temperature T_w is noted on the boundary of the sheet and T_∞ is the temperature away from the boundary. In the same way, $C_\infty$and C_w represent the concentrations at $y \to \infty$ and $y = 0$, respectively. The velocity $U_w(x) = u(x, 0) = cx$ is specified for the extending surface. The induced magnetic field components are expressed by $\vec{H_1}$ and $\vec{H_2}$ taken along and across the sheet, respectively. The subscript hnf signifies the hybrid nanofluid. The other terms involved in the system of equations (1)–(6) are specified in the nomenclature.

2.1 Preparation of pure (GO/EO) and hybrid nanofluids (Fe_3O_4–GO/EO)

The nano sized fragments of Fe_3O_4 and GO are mixed in the EO in order to prepare the hybrid mixture of Fe_3O_4–GO/EO. The nanoparticles volume fraction Fe_3O_4 (ϕ_1) is taken as 0.3 initially which is resolved in the base liquid (EO). After that amalgamation of GO (ϕ_2) in the solution of Fe_3O_4/EO leads toward the formation of hybrid nanofluids (Fe_3O_4–GO/EO). The fixed value of volume fraction Fe_3O_4 (*e.g.*, $\phi_1 = 0.3$) is taken throughout hereafter. The thermal properties of Fe_3O_4, GO, and EO are identified in Table 1. We have used these properties while analyzing the thermal and magnetic aspects of the problem. Further properties such as density, electrical conductivity, thermal conductivity, and specific heat (in either case of nanofluids) are taken from our earlier work (Ahmad *et al.* [28]). The notation s_1 signifies the nanoparticles volume fraction of Fe_3O_4 and s_2 is used for GO volume fraction. Whereas f is used for base fluid which is EO in the present case.

2.2 Dimensionless variables

We transmute the governing equations into dimensionless form by means of the following similarity variables:

Table 1: Thermal properties of graphene oxide, EO and Fe_3O_4

Properties	GO (s_2)	EO (f)	Fe_3O_4(s_1)
k (W/mK)	5,000	0.144	9.7
σ (s/m)	1.1×10^{-5}	2.1×10^{-12}	0.74×10^{6}
C_p (J/kgK)	717	1,910	670
ρ (kg/m^3)	1,800	884	5,180

$$\eta = \sqrt{\frac{c}{\upsilon_f}}y,\ \psi = \sqrt{c\upsilon_f}xf(\eta),\ \theta(\eta) = \frac{T - T_\infty}{T_w - T_\infty},$$
$$H_1 = H^* x g'(\eta),\ \phi(\eta) = \frac{C - C_\infty}{C_w - C_\infty}, \tag{7}$$
$$H_2 = -\sqrt{c\upsilon_f}\, g(\eta).$$

The relation (7) identically satisfies the continuity equation (1) and converts the equations (2)–(5) into the following form:

$$f''' = \Delta_1(f'^2 - ff'') + \Delta_2 M_0 f' + \beta\Delta_0(g'^2 - gg'' - 1), \tag{8}$$

$$\lambda_0\Delta_0 g''' + fg'' - gf'' = 0, \tag{9}$$

$$\frac{1}{\mathrm{Pr}}\Delta_3\theta'' + \Delta_4 f\theta' = 0, \tag{10}$$

$$\frac{1}{\mathrm{Sc}}\phi'' + f\phi' - \sigma(1 + \delta\theta)^{m1}\exp\left(\frac{-E_a}{1 + \delta\theta}\right)\phi = 0, \tag{11}$$

where

$$\Delta_0 = \frac{1}{\left[(1 - \phi_2)\left\{(1 - \phi_1) + \phi_1\frac{\rho_{s_1}}{\rho_f}\right\} + \phi_2\frac{\rho_{s_2}}{\rho_f}\right]}, \tag{12}$$

$$\Delta_1 = (1 - \phi_1)^{2.5}(1 - \phi_2)^{2.5}\left[(1 - \phi_2)\left\{(1 - \phi_1) + \phi_1\frac{\rho_{s_1}}{\rho_f}\right\} + \phi_2\frac{\rho_{s_2}}{\rho_f}\right], \tag{13}$$

$$\Delta_2 = (1 - \phi_1)^{2.5}(1 - \phi_2)^{2.5}\frac{\sigma_{\mathrm{hnf}}}{\sigma_f}, \tag{14}$$

$$\Delta_3 = \frac{K_{\mathrm{hnf}}}{K_f}, \tag{15}$$

$$\Delta_4 = \left[(1 - \phi_2)\left\{(1 - \phi_1) + \phi_1\frac{(\rho c_p)_{s_1}}{(\rho c_p)_f}\right\} + \phi_2\frac{(\rho c_p)_{s_2}}{(\rho c_p)_f}\right], \tag{16}$$

We have adopted almost similar process to formulate the relations (12)–(16) as in the references [29,30]. The boundary conditions given in (6) now become:

$$\left.\begin{array}{ll} \xi = 0: & f = S_0,\quad f' = 1,\quad \theta = 1,\quad \phi = 1,\quad H = 0, \\ \xi \to \infty: & f' \to 0,\quad \theta \to 0,\quad \phi \to 0,\quad H = 1. \end{array}\right\}. \tag{17}$$

2.3 The preeminent parameters

The preeminent parameters which are involved in the equations (8)–(11) and boundary conditions (17) are mentioned in Table 2.

Table 2: The preeminent parameters

$\delta = \frac{T_w - T_\infty}{T_\infty}$	Temperature difference parameter	$S_0 = \frac{v_0}{\sqrt{cv_f}}$	Suction parameter
$M_0^2 = \frac{\sigma_f B_0^2}{c\rho_f}$	Magnetic interaction parameter	$\mathrm{Pr} = \frac{\mu_f (c_p)_f}{k_f}$	Prandtl number
$C_R = \frac{K_r^2}{c}$	Chemical reaction rate constant	$\beta = \frac{\mu_e}{4\pi\rho_f}\left(\frac{H^*}{c}\right)^2$	Induced magnetic field parameter where H^* is the strength of uniformly induced magnetic field
$\lambda_0 = \frac{\eta_0}{v}$	Reciprocal magnetic Prandtl number where $\eta_0 = \frac{1}{4\pi\rho_f\mu_e}$ is the magnetic diffusivity	$E_0 = \frac{E^*}{k^* T_\infty}$	Activation energy parameter
$\mathrm{Sc} = \frac{v_f}{D_B}$	Schmidt number		

Further physical quantities, which belong to engineering interests such as Nusselt number, surface drag, and Sherwood number, are portrayed as:

$$\begin{aligned} \mathrm{Nu}_x \mathrm{Re}_x^{\frac{1}{2}} &= -\frac{k_{\mathrm{hnf}}}{k_f}\theta'(0), \\ \mathrm{Re}_x^{\frac{1}{2}} C_{fx} &= \frac{f''(0)}{(1-\phi_1)^{2.5}(1-\phi_2)^{2.5}}, \\ \mathrm{Sh}_x \mathrm{Re}_x^{\frac{1}{2}} &= -\phi'(0), \end{aligned} \tag{18}$$

Whereas the relation given by $\mathrm{Re}_x = \frac{U_w x}{v_f}$ represents the local Reynolds number.

3 Numerical scheme based on order reduction and finite difference discretization

The analytical solution of the nonlinear coupled differential equations (8)–(11) is not only difficult to find out but it might also consume an enormous time. However, numerical solution is the choice to develop the outcomes of the problem under consideration. A typical way is to alter the system in the 1st order system of ordinary differential equations whose solution might be determined using common numerical schemes. But, in this way, an inadequacy seems to appear in the case of missing conditions. The solution diverges sometimes even for precise guesses of missing conditions (*e.g.*, initial or boundary conditions). The strong dependence of the iterative process on the boundary conditions may be one of the reasons of this inconsistency. On the other hand, boundary conditions located at infinity can also interrupt the numerical solution. However, some efficient numerical technique is essentially required to tackle such types of troubles. The order reduction (*e.g.*, $z = f' = \frac{\mathrm{d}f}{\mathrm{d}\eta}$) together with finite difference discretization is adopted in our work to determine the numerical solution of the problem.

3.1 Discretization model

Initially, we reduced the order of equations (8) and (9) by substituting $z = f' = \frac{\mathrm{d}f}{\mathrm{d}\xi}$ and $s = g' = \frac{\mathrm{d}g}{\mathrm{d}\xi}$, respectively, and obtained

$$z'' = \Delta_1(z^2 - fz') + P_0 z + \Delta_2 M_0 z + \beta\Delta_0(g'^2 - gg'' - 1), \tag{19}$$

$$\lambda_0\Delta_0 s'' + fs' - gz' = 0. \tag{20}$$

In the same way, dimensionless energy and concentration equations (10) and (11) are

$$\frac{1}{\mathrm{Pr}}\Delta_3\theta'' + \Delta_4 f\theta' = 0, \tag{21}$$

$$\frac{1}{\mathrm{Sc}}\phi'' + f\phi' - \sigma(1+\delta\theta)^{m1}\exp\left(\frac{-E_a}{1+\delta\theta}\right)\phi = 0. \tag{22}$$

Now after using finite differences in the above equations, we obtain the following discretized equations:

$$\begin{aligned} &z_{i-1}(2 - h\Delta_1 f_i) + z_{i+1}(2 + h\Delta_1 f_i) \\ &\quad - z_i[4 + 2h^2(\Delta_1 z_i + \Delta_2 M_0 + P_0)] + A_3 = 0, \end{aligned} \tag{23}$$

where

$$A_3 = -\beta\Delta_0\left[\frac{1}{2}(g_{i+1} - g_{i-1})^2 - 2g_i(g_{i+1} - 2g_i + g_{i-1}) - 2h^2\right], \tag{24}$$

$$\begin{aligned} &\theta_{i-1}\left(\frac{2}{\mathrm{Pr}}\Delta_3 - hf_i\Delta_4\right) + \theta_{i+1}\left(\frac{2}{\mathrm{Pr}}\Delta_3 + hf_i\Delta_4\right) \\ &\quad - \left(\frac{4}{\mathrm{Pr}}\Delta_3\right)\theta_i = 0, \end{aligned} \tag{25}$$

$$\begin{aligned} &s_{i-1}(2\lambda_0\Delta_0 - hf_i) - 4\lambda_0\Delta_0 s_i \\ &\quad - 2g_i(f_{i+1} - 2f_i + f_{i-1}) + s_{i-1}(2\lambda_0\Delta_0 + hf_i) = 0, \end{aligned} \tag{26}$$

$$[4 + 2h^2 ScC_R e^{(E_{0/1+\delta})\theta(i)}((1+\delta)\theta_i)^{m_1}]\phi_i + \phi_{i-1}(2 - h\mathrm{Sc}f_i) + \phi_{i+1}(2 - h\mathrm{Sc}f_i) = 0, \quad (27)$$

We numerically solve the discretized equations (23)–(27). In our earlier work [31,32], we successfully implemented this technique to solve the complex nonlinear problems. The structure of this method (Figure 2) is such that it provides quick convergence and better execution.

Table 3: Change in heat transfer for different Prandtl numbers when $\phi_1 = \phi_2 = 0$

Pr	Devi and Devi [33]	Ali *et al.* [34]	Present results
2	0.91135	0.91045	0.91045
7	1.89540	1.89083	1.89083
20	3.35390	3.35271	3.35271
70	—	6.47814	6.47814

4 Comparison and error analysis

A numerical comparison, under certain conditions, is illustrated in Table 3. The comparison is found to be in good correlation with earlier ones and it appraises the efficiency of the code. Table 3 also predicts that an increase in heat transfer rate, for simple Newtonian case, is due to an increase in the values of the Prandtl number.

The convergence as well as error analysis is portrayed in Tables 4 and 5. These tables not only demonstrate the convergence and error analysis but also appraise the efficiency of code.

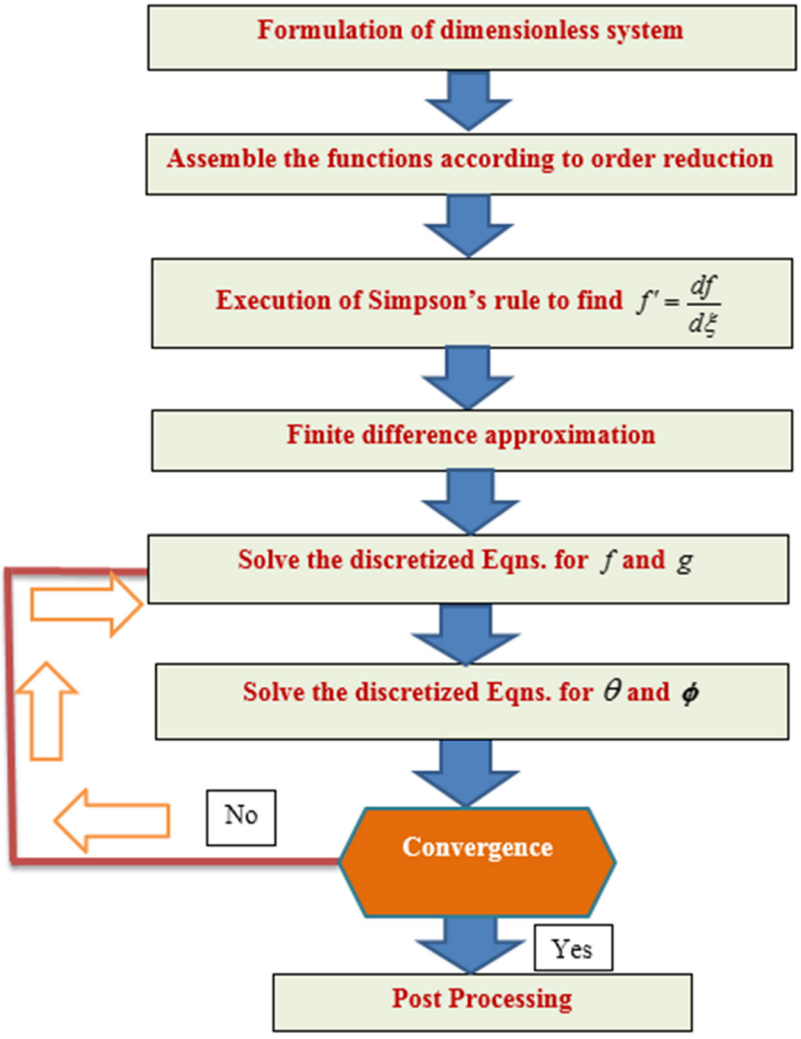

Figure 2: Structure of numerical algorithm.

Table 4: Convergence of numerical results for $f(\eta)$ with step-size η for $\beta_0 = 0.1$, $S_0 = 0.8$, $\lambda_0 = 3$, $M_0 = 2$, Pr = 6.135, $\delta = 4$, $m_0 = 3$, $\phi_2 = 0.08$, $\phi_1 = 0.3$, $\sigma_0 = 6$, $E_0 = 2$, Sc = 1

η	$f(\eta)$			
	$h = 0.07$	$h/2 = 0.035$	$h/4 = 0.0175$	$h/8 = 0.00825$
0	0.80000000	0.80000000	0.80000000	0.80000000
0.7	1.12768459	1.12760689	1.12758767	1.12758288
1.4	1.18113888	1.18101728	1.18098709	1.18097956
2.1	1.18812018	1.18798486	1.18795126	1.18794287
2.8	1.18789295	1.18775271	1.18771789	1.18770920
3.5	1.18696821	1.18682553	1.18679011	1.18678127
4.2	1.18626526	1.18612106	1.18608527	1.18607634
4.9	1.18581247	1.18566728	1.18563126	1.18562226
5.6	1.18553611	1.18539032	1.18535414	1.18534512
6.3	1.18538022	1.18523418	1.18519791	1.18518886
7.0	1.18532408	1.18517832	1.18514204	1.18513298

Table 5: Change in error for $f(\eta)$ with step-size η for $\beta_0 = 0.1$, $S_0 = 0.8$, $\lambda_0 = 3$, $M_0 = 2$, Pr = 6.135, $\delta = 4$, $m_0 = 3$, $\phi_2 = 0.08$, $\phi_1 = 0.3$, $\sigma_0 = 6$, $E_0 = 2$, $Sc = 1$

(**Absolute change in error with step-size h**) $\times 10^{-3}$			
η	h to $h/2$	$h/2$ to $h/4$	$h/4$ to $h/8$
0	0	0	0
0.7	0.0777	0.0192	0.0047
1.4	0.1216	0.0301	0.0075
2.1	0.1353	0.0336	0.0083
2.8	0.1402	0.0348	0.0086
3.5	0.1426	0.0354	0.0088
4.2	0.1442	0.0357	0.0089
4.9	0.1451	0.0360	0.0089
5.6	0.1457	0.0361	0.0090
6.3	0.1460	0.0362	0.0090
7.0	0.1457	0.0362	0.0090

5 Results and discussion

The main focus, in this section, is to explore the novel aspects of the prime parameters for the flow of usual as well as hybrid case of nanofluids. The pure nanofluid case is assumed by taking the nanocomposites of GO with the base fluid which is EO in the present case. Likewise, hybrid case of nanofluids (*e.g.*, GO–Fe_3O_4/EO) is also taken into account. In this way, features of both pure and hybrid case of nanofluids are covered in this work. Assigning distinct values to the parameters, instead of particular values, may provide better results in factual applications of the work. The specified values of parameters in the numerical calculations are: Pr = 6.135, $\delta = 4$, $m_0 = 3$, Sc = 1 and the other values are given in Tables 6 and 7.

The impact of induced magnetic field parameter β_0 is portrayed in Figure 3 which describes the variation in velocity and induced magnetic field of pure GO–EO nanofluid and hybrid GO–Fe_3O_4/EO nanofluid. An induced magnetism can be generated in hybrid nanofluids by the magnetic dipole due to which induced current will vary. This phenomenon tends to reduce the induced magnetic field as well as velocity. This nature of the parameter β_0 makes the hybrid nanofluid (GO–Fe_3O_4/EO) much useful in photo-catalytic and semiconductors technology. Figure 4 shows the appearance of velocity $F'(\xi)$ and temperature $\theta(\xi)$ (as a function of η) for distinct values of suction parameter. These figures evidently reveal that the velocity as well as temperature of the fluid turns toward reduction in either case of nanofluid (pure and hybrid case).

Table 6 portrays the change in Nusselt numbers and Shear stresses against various parameters for both cases of nanofluids *e.g.,* pure and hybrid nanofluid case. It has been noticed here that both the shear stress and Nusselt number tend toward enhancement due to the suction on the surface. Suction phenomenon generates a frictional force between fluid's particles and surface due to which shear rate increases in both cases of nanofluids. The optimal solution interrupts when we assign large values to the suction parameter. However, the small values of this parameter (*i.e.*, $S_{uc} < 1.0$) lead the solution toward the stability and we obtain better convergence. The heat transport rate decreases steadily with the impact of applied magnetic field but its effect is to marginally increase the shear rate on the sheet surface. The hybrid nanofluid GO–Fe_3O_4/EO has a substantial effect on shear stress with the effect of applied magnetic field as compared to usual nanofluid which can be evidently observed from

Table 6: Change in $\mathrm{Re}_x^{1/2}C_f$ and $\mathrm{Re}_x^{-1/2}\mathrm{Nu}_x$ for GO/EO and GO − Fe_3O_4/EO

Values of parameters				Shear stresses		Nusselt numbers	
β_0	S_0	λ_0	M_0	GO/EO	GO−Fe_3O_4/EO	GO/EO	GO−Fe_3O_4/EO
0.3	0.8	3	1.2	−2.63194	−5.75363	5.66258	7.81165
0.6				−2.91135	−6.00177	5.62881	7.78157
0.9				−3.21293	−6.26116	5.58908	7.74856
1.2				−3.54698	−6.53337	5.53938	7.71197
0.3	1.5	3	1.2	−3.15478	−6.84054	9.52567	12.77747
	2.0			−3.55727	−7.69149	12.31918	16.42816
	2.5			−3.97801	−8.59631	15.09426	20.10754
	3.0			−4.41304	−9.54678	17.83080	23.78906
0.3	0.8	0.3	1.2	−2.33067	−5.31521	5.70340	7.87497
		0.5		−2.45395	−5.42635	5.68749	7.86184
		0.7		−2.51665	−5.50215	5.67898	7.85169
		0.9		−2.55301	−5.55778	5.67392	7.84364
0.3	0.8	3	0	−2.07525	−4.15984	5.70846	7.95729
			4	−5.62316	−13.10718	5.46481	7.33720
			8	−10.31007	−24.26423	5.27579	6.97005
			12	−14.83891	−35.03407	5.16745	6.78365

Table 7: Change in $\mathrm{Re}_x^{-1/2}\mathrm{Nu}_x$ and $\mathrm{Re}_x^{-1/2}\mathrm{Sh}_x$ for GO/EO and GO−Fe_3O_4/EO

	Values of parameters			Nusselt numbers		Sherwood numbers	
ϕ_2	ϕ_1	C_R	E_0	GO/EO	GO−Fe_3O_4/EO	GO/EO	GO−Fe_3O_4/EO
0.03	0.3	6	2	5.65065	7.82174	—	—
0.06				5.66274	7.81962		
0.09				5.67559	7.81842		
0.12				5.68948	7.81843		
0.08	0.1	6	2	6.32993	6.46176	—	—
	0.2			7.05333	7.17728		
	0.3			7.82612	8.00156		
	0.4			8.67174	8.99314		
0.08	0.3	0	2			1.11473	1.14216
		1				5.79774	7.08680
		3				11.44395	12.96163
		5				15.09251	16.59830
0.08	0.3	6	3			14.67421	16.30981
			5			11.19862	13.09641
			7			8.22614	10.21281
			9			5.90833	7.72788

Table 6. The surface drag $\mathrm{Re}_x^{1/2}C_f$ seems to increase and that of Nusselt number $\mathrm{Re}_x^{-1/2}\mathrm{Nu}_x$ decrease provided the values of magnetic Prandtl number and induced magnetic field parameter β_0 increase, respectively (Table 6). Both these parameters act parallel to each other in case of their effects on shear rates and heat transfer rates. A significant change in the values of Nusselt number is noticed with the effect of suction parameter whereas the other parameters have low effect on it.

The increasing values of the magnetic Prandtl number λ_0 cause a substantial reduction in the velocity and induced magnetic field for both the usual and hybrid case of nanofluids, as shown in Figure 5a and b. The magnetic field strength reduces with lower magnetic diffusivity which mainly causes the reduction in induced magnetic field and velocity. It has been noticed from the consequences of Figure 6a and b that the influence of magnetic field M_0 is to dissuade the velocity and to escalate the

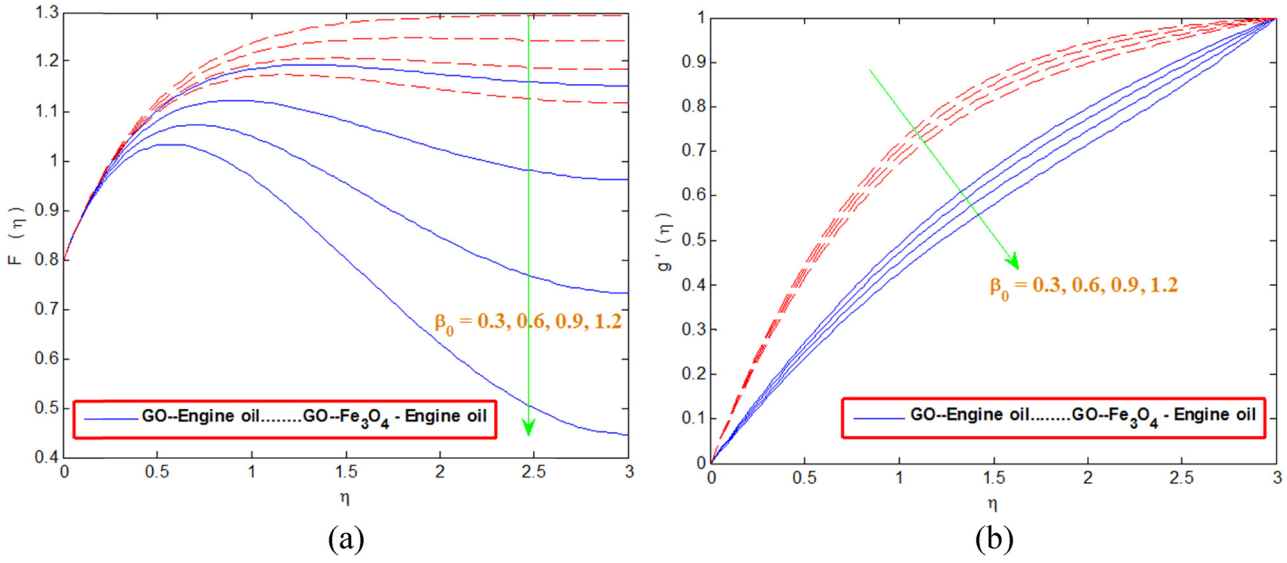

Figure 3: Change in (a) velocity and (b) induced magnetic field with β_0.

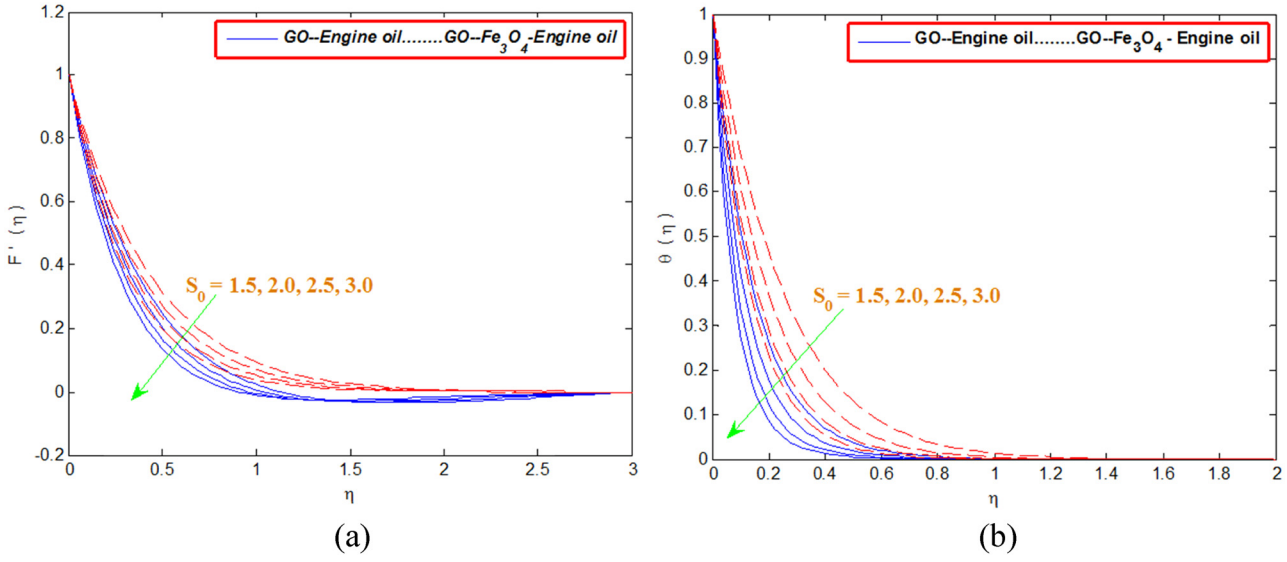

Figure 4: Change in (a) velocity and (b) temperature with S_0.

temperature for same grid size (η). The magnetic retardation force caused by the Lorentz force tends to raise the temperature and ultimately increases the thermal boundary layer thickness. Contrarily, it causes diminution in the thickness of momentum boundary. It is important to mention here that the hybrid nanofluid GO–Fe_3O_4/EO performs well in case of temperature enhancement as compared to mono nanofluid GO/EO.

The GO nanoparticles volume fraction ϕ_2 and Fe_3O_4 nanoparticles volume fraction ϕ_1 have a significant impact on the thermal features of both pure and hybrid nanofluids. Obviously, the base fluids enriched with the nanoparticles can embellish the thermal characteristics in many industrial applications. However, the desired heat transfer rate can be achieved by the amalgamation of hybrid nano-composites into the base liquids. The hybrid nano-composites GO–Fe_3O_4/EO increase temperature more rapidly whereas mono nano-composites GO/EO (ϕ_2) has low effect on temperature as pictured in Figure 7a. It has been comparatively noticed from Figure 7a and b that the solid nanoparticles volume fraction ϕ_1 of Fe_3O_4 nanoparticles increases temperature more efficiently than solid nanoparticles volume fraction ϕ_2 of GO nanoparticles. In Figure 7b, it is important to mention

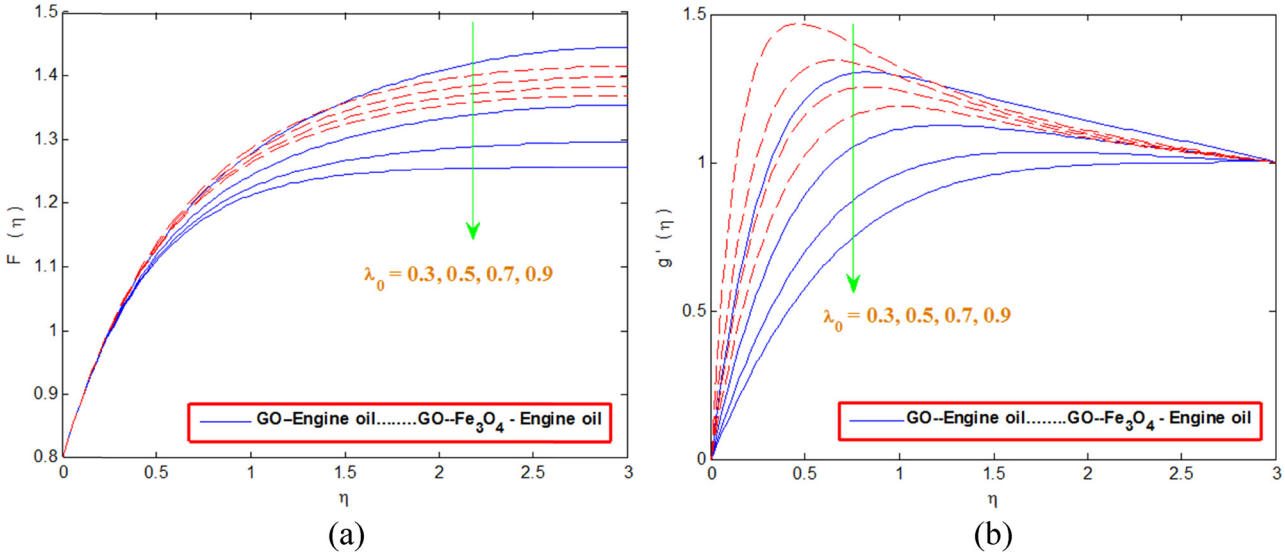

Figure 5: Change in (a) velocity and (b) induced magnetic field with λ_0.

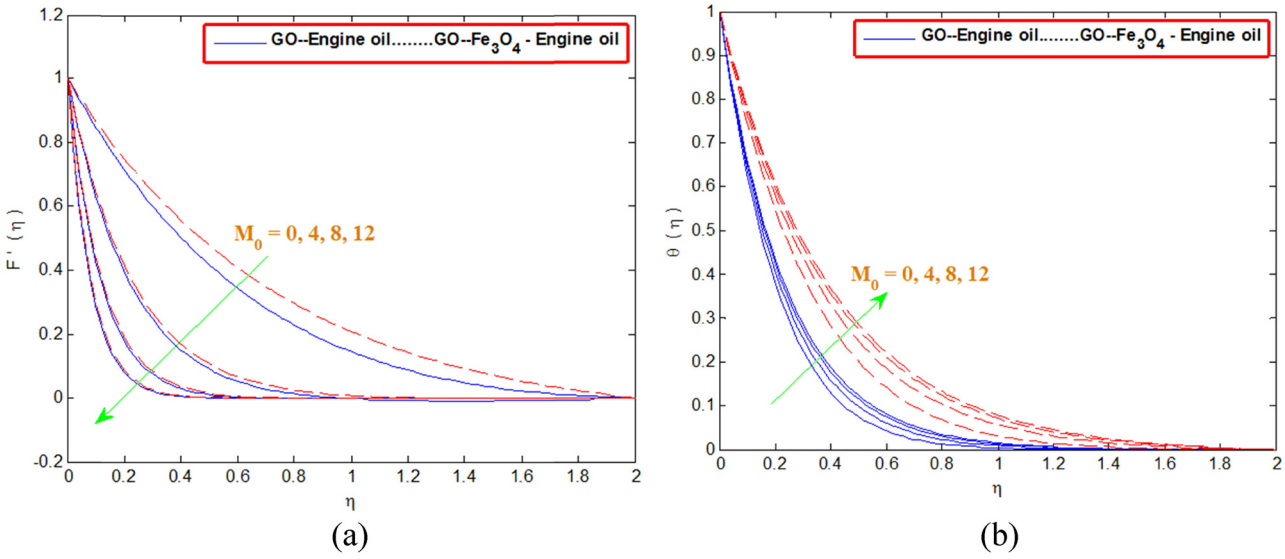

Figure 6: Change in (a) velocity and (b) temperature with M_0.

that $\phi_2 = 0$ for pure nanofluid case GO/EO whereas $\phi_2 = 0.3$ in hybrid case GO–Fe_3O_4/EO.

The analysis of heat and mass transfer rates for several parameters like nanoparticles volume fraction, activation energy, and chemical reaction parameter is provided in Table 7. The nanoparticles volume fraction ϕ_2 shows a reduction in heat transfer rate when hybrid case of nanofluids (GO–Fe_3O_4/EO) is considered but it causes an enhancement in the rate of heat transfer in case of pure nanofluid (GO/EO). It is worth observing here that heat transfer rate reduces gradually for GO–Fe_3O_4/EO with the effect of volume fraction ϕ_2 whereas heat transfer rates elevate in case of GO/EO. In the same way, the effect of solid nanoparticles volume fraction ϕ_1 of Fe_3O_4 is to enhance the heat transfer rate in both the cases of nanofluids. However, it is concluded that the mixture of hybrid nano-composites such as GO and Fe_3O_4 together with EO can be used as coolant/heating agents to cool down or heat up the systems. Therefore, the present results may be applied (with caution) to thermal cooling/heating systems. The heat transfer rate over a surface is important in order to attain the required consequences. The impact of activation energy is to devaluate the rate of mass transfer but contrarily the chemical reaction parameter sufficiently

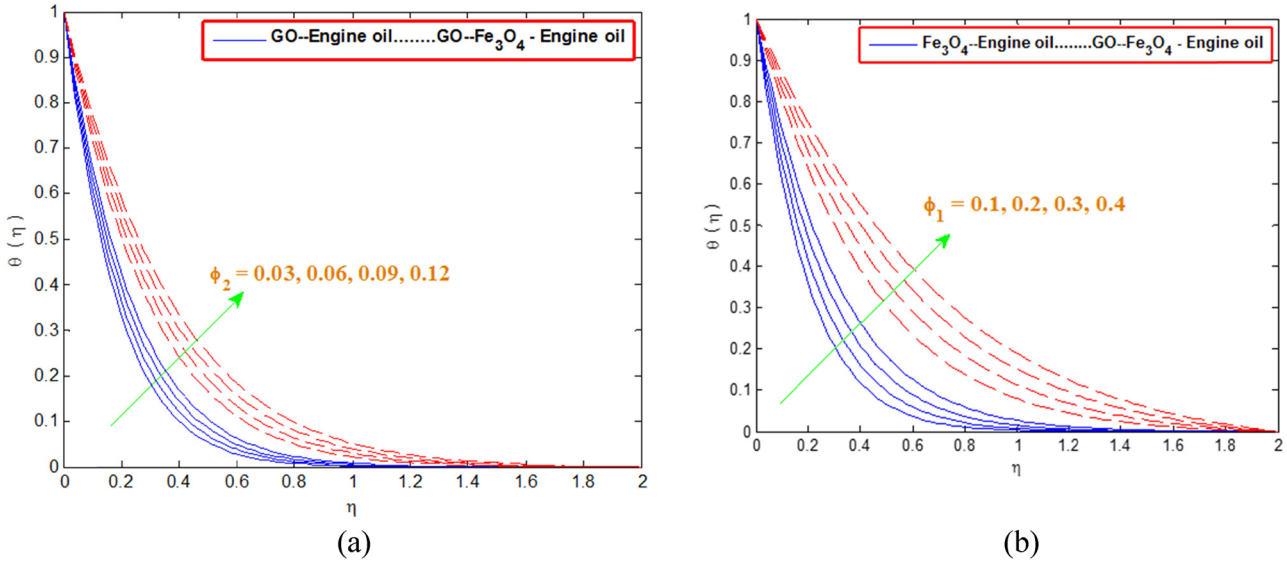

Figure 7: Change in temperature with (a) volume fraction ϕ_2 and (b) volume fraction ϕ_1.

enhances the mass transfer rate on the surface of sheet, as depicted in Table 7. The increasing values of activation energy parameter modify the Arrhenius function which causes a reduction in mass transfer.

The concentration curves, against chemical reaction and activation energy parameter, demonstrate an adversative trend for hybrid and usual case of nanofluids with EO as host fluid (Figure 8a and b). The minimum amount of energy required to accelerate a chemical reaction process is known as activation energy. However, the inflate concentration is associated with the large values of activation energy E_0. This fact is attributed by the Arrhenius equation which states that the higher will be the activation energy, the higher will be the concentration. On the opposite side, the chemical reaction parameter causes a deceleration in the concentration. Flow is more concentrated for GO–Fe_3O_4/EO as equated to GO/EO.

6 Conclusion

Some industrial and engineering processes *e.g.*, nuclear system cooling, metal expulsion, cooling generator, solar

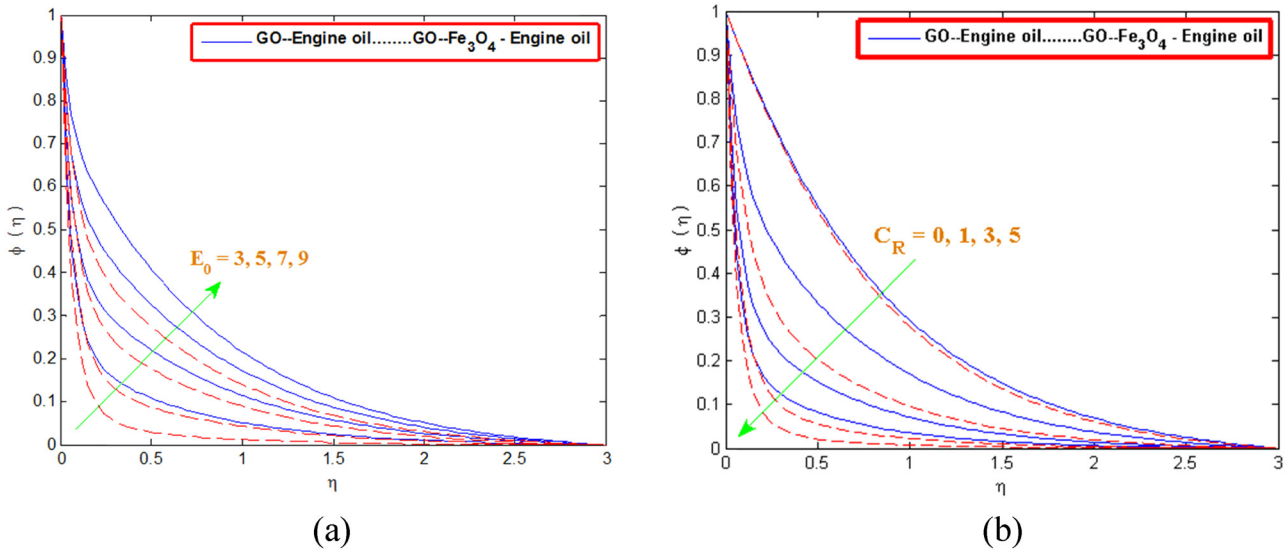

Figure 8: Change in concentration with (a) chemical reaction parameter and (b) activation energy.

heating, thermal storage, refrigeration, and so forth demand a specific rate of heat which could not affect the ultimate quality or final worth of the product. Heat transfer rate can be managed using hybrid mixture of Fe_3O_4 and GO in EO which can provide assistance in acquiring better quality products at low cost. Moreover, use of induced magnetic field not only regulates the flow but it also controls the variation in the flow. In the same way, magnetic effect maintains the thermal properties in several dynamical phenomena. We have investigated, in the recent work, the thermal and flow features of mono nanofluid GO/EO and hybrid nanofluid Fe_3O_4–GO/EO under the induced magnetic field environment. Finite difference discretization together with order reduction method is used to acquire the simulated outcomes. The prime findings of the problem under consideration may be listed as follows:

- The magnetic Prandtl number λ_0 causes a substantial reduction in the induced magnetic field and velocity for both GO/EO (nanofluid case) and Fe_3O_4–GO/EO (hybrid nanofluid case).
- Both the shear stress and Nusselt number tend toward enhancement on the surface due to the suction whereas temperature and fluid motion decreased in the flow regime with suction phenomenon.
- An increase in the concentration is due to the effect of activation energy whereas the decrease in concentration is due to chemical reaction.
- The temperature seems to be elevating but Nusselt number decreases with the impact of applied magnetic field.
- The nanoparticles volume fraction ϕ_2 causes an enhancement in the rate of heat transfer in case of pure nanofluid (GO/EO) but it shows a reduction in heat transfer rate in the case of hybrid nanofluids (GO–FE_3O_4/EO).
- The temperature is accelerated with the effect of volume fraction ϕ_2 of GO in case of usual and hybrid nanofluids.

Acknowledgments: The researchers would like to thank the Deanship of Scientific Research, Qassim University for funding the publication of this project.

Funding information: The project was funded by the Deanship of Scientific Research, Qassim University.

Author contributions: All authors have accepted responsibility for the entire content of this manuscript and approved its submission.

Conflict of interest: The authors state no conflict of interest.

Data availability statement: The datasets generated during and/or analysed during the current study are available from the corresponding author on reasonable request.

References

[1] Shah Z, Saeed A, Khan I, Selim MM, Ikramullah, Kumam P. Numerical modeling on hybrid nanofluid (Fe_3O_4 + MWCNT/H_2O) migration considering MHD effect over a porous cylinder. PLoS One. 2021;16(7):e0251744.

[2] Tekir M, Taskesen E, Gedik E, Arslan K, Aksu B. Effect of constant magnetic field on Fe_3O_4-Cu/water hybrid nanofluid flow in a circular pipe. Heat Mass Transfer. 2022;58:707–17.

[3] Ahmad S, Akhter S, Shahid MI, Ali K, Akhtar M, Ashraf M. Novel thermal aspects of hybrid nanofluid flow comprising of manganese zinc ferrite $MnZnFe_2O_4$, nickel zinc ferrite $NiZnFe_2O_4$ and motile microorganisms. Ain Shams Eng J. 2022;13(5):101668.

[4] Aristizabal-Fontal JE, Corte´s FB, Franco CA. Viscosity reduction of extra heavy crude oil by magnetite nanoparticle-based ferrofluids. Adsorpt Sci Technol. 2018;36(1–2):23–45.

[5] Astafyev A, Lysenko E, Surzhikov A, Nikolaev E, Vlasov V. Thermomagnetometric analysis of nickel–zinc ferrites. J Therm Anal Calorim. 2020;142:1775–81.

[6] Hemmat Esfe M, Alidoust S, Mohammadnejad Ardeshiri E, Kamyab MH, Toghraie D. Experimental study of rheological behavior of MWCNT-Al_2O_3/SAE50 hybrid nanofluid to provide the best nano-lubrication conditions. Nanoscale Res Lett. 2022;17:4.

[7] Vidhya R, Balakrishnan T, Suresh Kumar B, Palanisamy R, Panchal H, Angulo-Cabanillas L, et al. An experimental study of ZrO_2-CeO_2 hybrid nanofluid and response surface methodology for the prediction of heat transfer performance: The New Correlations. J Nanomater. 2022;2022:1–11. doi: 10.1155/2022/6596028.

[8] Yalçın G, Öztuna S, Dalkılıç AS, Nakkaew S, Wongwises S. An experimental study on SiO_2-ND hybrid nanofluid: thermal conductivity, viscosity, and stability with new forecast models. Curr Nanosci. 2022;18(6):520–34. doi: 10.2174/1573413718666220111103031.

[9] Mishra A, Upreti HA. Comparative study of Ag–MgO/water and Fe_3O_4–Co Fe_2O_4/EG–water hybrid nanofluid flow over a curved surface with chemical reaction using Buongiorno model. Partial Differ Equ Appl Math. 2022;5:100322.

[10] Jan WU, Farooq M, Khan A, Alharbi A, Ali Shah R, Jan R, et al. A Parametric Analysis of the Effect of Hybrid Nanoparticles on the Flow Field and Homogeneous-Heterogeneous Reaction between Squeezing Plates, A parametric analysis of the effect of hybrid nanoparticles on the flow field and homogeneous-heterogeneous reaction between squeezing plates. Adv Math Phy. 2022;2022:2318436–22. doi: 10.1155/2022/2318436.

[11] Ali K, Faridi AA, Ahmad S, Jamshed W, Khan N, Alam MM. Quasi-linearization analysis for heat and mass transfer of magnetically driven 3rd-grade (Cu-TiO_2/engine oil) nanofluid *via* a convectively heated surface. Int Commun Heat Mass Transfer. 2022;135:106060.
[12] Yu Q, Su Y, Tursun R, Zhang J. Synthesis and characterization of low density porous nickel zinc ferrites. RSC Adv. 2019;9:13173–81.
[13] Azhagushanmugam SJ, Suriyanarayanan N, Jayaprakash R. Effect of cation distribution on structural and magnetic properties of Nickel Cobalt Zinc Ferrites. Adv Mater Sci Eng. 2013;713684. doi: 10.1155/2013/713684.
[14] Al-Sankoor K, Al-Gayyim H, Al-Musaedi S, Asadi Z, Ganji DD. Analytically investigating of heat transfer parameters with presence of graphene oxide nanoparticles in Williamson-magnetic fluid by AGM and HPM methods. Case Stud Therm Eng. 2021;27:101236.
[15] Hosseinzadeh S, Hosseinzadeh KhHasibi, Ganji A, DD. Hydrothermal analysis on non-Newtonian nanofluid flow of blood through porous vessels. Proc Inst Mech Eng E J Process Mech Eng. 2022;236(4):1604–15. doi: 10.1177/09544089211069211.
[16] Talebi Rostami H, Fallah Najafabadi M, Hosseinzadeh Kh, Ganji DD. Investigation of mixture-based dusty hybrid nanofluid flow in porous media affected by magnetic field using RBF method. Int J Ambient Energy. 2022;1–11. doi: 10.1080/01430750.2021.2023041.
[17] Fallah Najafabadi M, Talebi Rostami H, Hosseinzadeh Kh, Ganji DD. Thermal analysis of a moving fin using the radial basis function approximation. Heat Transfer. 2021;50(8):7553–67.
[18] Alaraji A, Alhussein H, Asadi Z, Ganji DD. Investigation of heat energy storage of RT26 organic materials in circular and elliptical heat exchangers in melting and solidification process. Case Stud Therm Eng. 2021;28:101432.
[19] Hosseinzadeh S, Hosseinzadeh Kh, Hasibi A, Ganji DD. Thermal analysis of moving porous fin wetted by hybrid nanofluid with trapezoidal, concave parabolic and convex cross sections. Case Stud Therm Eng. 2022;30:101757.
[20] Hosseinzadeh KH, Roghani S, Mogharrebi AR, Asadi A, Waqas M, Ganji DD. Investigation of cross-fluid flow containing motile gyrotactic microorganisms and nanoparticles over a three-dimensional cylinder. Alexandria Eng J. 2020;59(5):3297–3307.
[21] Bestman AR. Natural convection boundary layer with suction and mass transfer in porous medium. Int J Eng Res. 1990;14:389–96.
[22] Ramesh GK, Madhukesh JK. Activation energy process in hybrid CNTs and induced magnetic slip flow with heat source/sink. Chinese J Phy. 2021;73:375–90.
[23] Madhukesh JK, Ramesh GK, Roopa GS, Prasannakumara BC, Shah NA, Yook SJ. 3D flow of hybrid nanomaterial through a circular cylinder: Saddle and Nodal Point Aspects. Mathematics. 2022;10:1185.
[24] Almaneea A. Numerical study on heat and mass transport enhancement in MHD Williamson fluid *via* hybrid nanoparticles. Alex Eng J. 2022;61(10):8343–54.
[25] Rekha MB, Sarris IE, Madhukesh JK, Raghunatha KR, Prasannakumara BC. Activation energy impact on flow of AA7072-AA7075/water-based hybrid nanofluid through a cone, wedge and plate. Micromachines. 2022;13(2):302.
[26] Ahmad S, Ali K, Rizwan M, Ashraf M. Heat and mass transfer attributes of copper-aluminum oxide hybrid nanoparticles flow through a porous medium. Case Stud Therm Eng. 2021;25:100932.
[27] Gireesha BJ, Mahanthesh B, Shivakumara IS, Eshwarappa KM. Melting heat transfer in boundary layer stagnation-point flow of nanofluid toward a stretching sheet with induced magnetic field. Int J Eng Sci Technol. 2016;19:313–21.
[28] Ahmad S, Ali K, Ashraf M. MHD flow of Cu-Al_2O_3/water hybrid nanofluid through a porous media. J Por Media. 2021;24(7):61–73.
[29] Suriya Uma Devi S, Anjali, Devi SP. Heat transfer enhancement of Cu-Al_2O_3/water hybrid nanofluid flow over a stretching sheet. J Niger Math Soc. 2017;36:419–33.
[30] Waini I, Ishak A, Pop I. Hybrid nanofluid flow and heat transfer past a permeable stretching/shrinking surface with a convective boundary condition. J Phy Conf Ser. 2019;1366:012022.
[31] Ahmad S, Younis J, Ali K, Rizwan M, Ashraf M, Abd El Salam MA. Impact of swimming gyrotactic microorganisms and viscous dissipation on nanoparticles flow through a permeable medium- A numerical assessment. J Nanomaterials. 2022;4888128. doi: 10.1155/2022/4888128.
[32] Ahmad S, Ashraf M, Ali K. Bioconvection due to gyrotactic microbes in a nanofluid flow through a porous medium. Heliyon. 2020;6:e05832.
[33] Devi SPA, Devi SSU. Numerical investigation of hydromagnetic hybrid Cu-Al_2O_3/water nanofluid flow over a permeable stretching sheet with suction. Int J Nonlin Sci Numer Simul. 2016;17(5):249–57.
[34] Ali K, Ahmad S, Nisar KS, Faridi AA, Ashraf M. Simulation analysis of MHD hybrid Cu-Al_2O_3/H_2O nanofluid flow with heat generation through a porous media. Int J Energy Res. 2021;45(13):19165–79. doi: 10.1002/er.7016.